Chapter 5
Quantum Aspects of Biophotonics

Jean-Pierre Wolf

5.1 Introduction

Interestingly, while adopted for a long time in the particle physics community as a usual gauge boson, the *photon*, i.e. the quantum particle associated with light, is still sometimes debated in the *photonics* community. Some weird questions are associated, like "is this photonic process quantum?", "is it purely quantum?" or "is it non-trivially quantum?". In the present chapter, we will not enter these discussions, but rather consider processes in which the state of a system is in a quantum superposition of different states (e.g. a Schroedinger cat) or in which distinct subsystems are entangled (via non-locality).

Even more debated is the emerging field of quantum biology [1] in which some quantum pathways are supposed to be chosen in the process of natural evolution. A pivotal work was performed in 2007 by G. Fleming [2], in which he demonstrated that quantum coherent energy transfer takes place in some photosynthetic systems. More precisely, he studied by 2D-spectroscopy the light harvesting process of the green-sulphur bacteria, which has an efficiency of almost 100% for transferring the energy of an absorbed photon to the reaction center. This amazing efficiency is achieved via a specialized molecular structure called Fenna-Matthews-Olson (FMO) complex. The time resolved 2D spectra clearly showed quantum coherences between excitons from multiple pigments within the FMO structure. These results were originally obtained at 77 K, but further investigations showed that partial coherence survives, even at room temperature [3]. A major question however remains: although existing, do these quantum superpositions of states play a major

J.-P. Wolf (✉)
GAP-Biophotonics, University of Geneva, Geneva, Switzerland
e-mail: jean-pierre.wolf@unige.ch

B. Di Bartolo et al. (eds.), *Quantum Nano-Photonics*, NATO Science for Peace and Security Series B: Physics and Biophysics,
https://doi.org/10.1007/978-94-024-1544-5_5

role and are they used by Nature to enhance the efficiency of harvesting light beyond the classical limits? These questions remain open today, and are actively debated in the literature.

A particular field that uses the dynamics of quantum superpositions of states is quantum coherent control. The aim, in this case, is to optimize the efficiency of some photo-biological processes, e.g. vision, by shaping the interacting laser field. We will dedicate a significant part of this chapter to coherent control methods and applications in biophotonics.

After an introduction of the basic processes and techniques used in coherent control, such as quantum pathways interference, we will concentrate on recent achievements in the field of coherent manipulation of biological objects. Particular interest will be dedicated to the identification of biological molecules that exhibit almost identical linear spectra and the wealth of related applications, such as specific serum proteins and pathogen detection. We show that by playing with quantum interference between reaction pathways, it is possible to discriminate nearly identical cellular vitamins [4, 5] and identify selectively proteins (antibodies) in blood serum. Immunoglobulins G and M, as well as albumin, could be directly be quantified in blood serum label-free, yielding the first "Quantum Control Based Bio-assays" [6].

5.2 Basics of Coherent Quantum Control

Coherent quantum control had a significant impact on photochemistry and spectroscopy. Not only could the atomic motion be *observed* within molecules by snapshots of a few femtoseconds duration, it could also be *controlled*. The basic idea of this revolution is the use of quantum interference between different states that are in coherent superposition so that a target state is reached with maximum probability. The mechanism reminds interference in optics, where some optical paths are favored (constructive interference) while others are discarded (destructive interference), as in Young's double slit experiment. A key element for achieving this control is the transfer of coherence from the exciting light field to the atomic or molecular system via the electric dipole operator. A tailored coherent laser pulse is used to excite a molecule in a superposition of states, which drives the molecule along a specific path to obtain a targeted result.

A famous example of coherent control is the Tannor, Koslov and Rice [7, 8] "pump-dump" method (Fig. 5.1), in which many vibrational states of a molecule ABC are coherently excited for generating a vibrational wavepacket. This wavepacket explores, as a function of time, a large fraction of the electronically excited hypersurface. By firing a second laser at convenient times t1 or t2, the molecule is brought back to its ground state but onto different dissociation paths, resulting in different species AB + C or A + BC. The system can thus be driven to a specific fragment by using the quantum control of the photodissociation process.

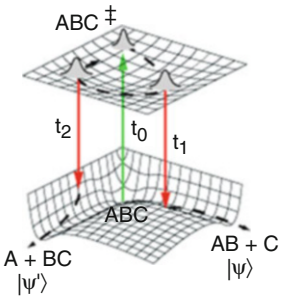

Fig. 5.1 Coherent control of the dissociation pathways of the molecule "ABC " [7, 8]

In 1992, H. Rabitz at Princeton introduced [9, 10] the concept of "optimal control", in which a feedback loop optimizes the laser pulse characteristics to reach most efficiently the desired target. For this, a large number of parameters (corresponding to the amplitude and phase of each spectral component within the exciting laser spectrum) have to be controlled. This "pulse shaping" technique is usually performed by introducing a liquid crystal array in the Fourier plane between two gratings (4f arrangement) [11]. Excellent results in terms of efficiency have been obtained using genetic-type optimization algorithms [12].

Besides the above mentioned "pump-dump" scheme, other successful control methods have been extensively applied, including stimulated Raman scattering (STIRAP), Four Wave Mixing like CARS (Coherent AntiStokes Raman Scattering), multiphoton absorption and multiphoton ionization. For more information about general quantum control aspects, a detailed review article has been published by M. Dantus et al. [13]. The controlled targets can be, for instance, specific fragments, specific isomers or specific isotopes, but also the enhancement or reduction of the fluorescence of a specific molecule (by driving it preferentially into other relaxation pathways). In this respect, a pioneering work has been performed by the group of G. Gerber [14, 15], in which the capability of distinguishing two different dyes using 2-photon absorption control was demonstrated, although the dyes had similar linear absorption and fluorescence spectra.

Experiments based on quantum control in biology have also been performed. Some striking examples are the control of the relaxation pathways in rhodopsin complexes [16, 17], the vibrational CO ladder climbing in hemoglobin [18] and pH-sensitive measurements in multi-photon microscopy [19].

An attractive application is the ability of discriminating different biological systems that are usually undistinguishable with standard linear spectroscopic approaches. One can think for instance to the early detection of cancer using the detection of specific proteins, the label-free monitoring of the cell metabolism, or the detection and identification of harmful bacteria. The aim of this chapter is to discuss these potential applications of quantum control (Fig. 5.2).

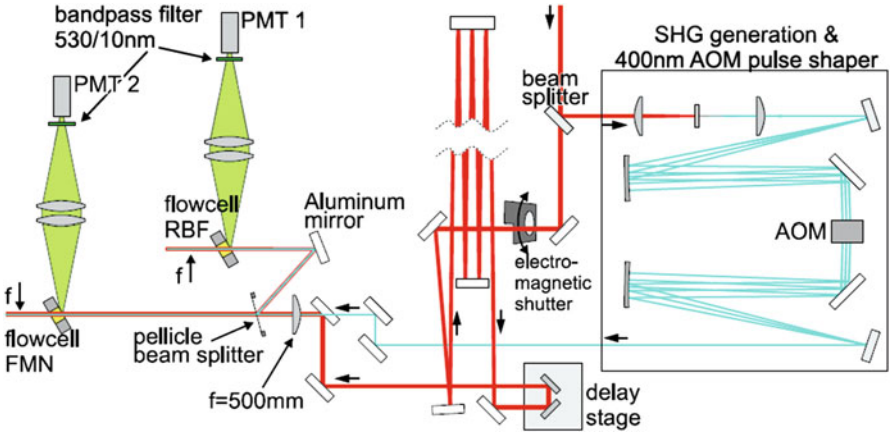

Fig. 5.2 Experimental implementation of the quantum control based optimal discrimination of two flavins (RBF and FMN). The experiment relies on fluorescence depletion with an optimally shaped excitation laser pulse. The pulse shaper uses a 4f line and an acousto-optic modulator (AOM). (From Ref. [4])

5.3 Use of Optimal Quantum Control for Discriminating Almost Identical Bio-molecules

The identification or discrimination of molecules and quantum systems that are nearly identical (proteins, bacteria, etc..) is normally an exceedingly difficult task. The conventional means of addressing this common need is through various *static* spectroscopic techniques, which can be especially difficult in complex remote environments. However, recent theoretical work showed that two or more quantum systems, even if they differ only infinitesimally, may be drawn apart to have distinct signatures through tailored control of their *dynamics*. Ultrafast broad bandwidth lasers with adaptive pulse shaping provide a means to implement this theoretical concept through controlled quantum optimal dynamic discrimination (ODD) [20]. In collaboration with the group of H. Rabitz at Princeton University, we demonstrated the capabilities of ODD by discriminating between two almost identical molecules of riboflavin (RBF) and flavin mononucleotide (FMN) in water solution, which have virtually identical linear absorption and fluorescence spectra (see Fig. 5.3a, b) [4, 5]. The successful implementation of ODD opens up numerous applications including in fluorescence microscopy, protein identification, as well as possible remote discrimination of different bacteria. A key component of ODD is operation with shaped laser pulses, which can nonlinearly interact with the molecules to fully exploit their dynamical capabilities and create discriminating signatures. The similar optical spectra of RBF and FMN arise from the common isoalloxazine ring with the only distinguishing feature being changes at the end of the side chain tail (Fig. 5.3a).

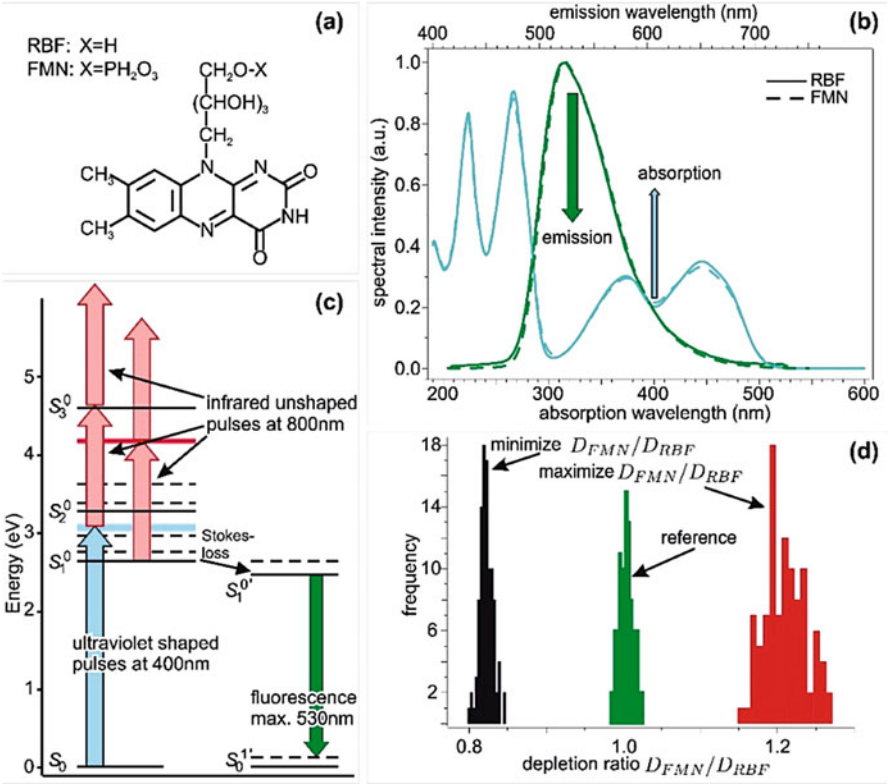

Fig. 5.3 The RBF and FMN molecules in (**a**) are very similar exhibiting nearly identical linear absorption and emission spectra in (**b**). The shaped UV control is centred at 400 nm and the flavin fluorescence signals are recorded over a window around 530 nm indicated by the respective arrows. The controlled optimal dynamic discrimination (ODD) of the flavins operates as indicated in (**c**) with a shaped UV pulse coordinated with a time delayed unshaped IR pulse to draw apart the vibronic dynamics of the flavins in the S_1 or S_2 excited states. The unshaped IR pulse serves to selectively disrupt the subsequent fluorescence signals from the two flavins and the red arrows indicate various possible means of action for the IR pulses. A typical outcome is shown in (**d**) where the ratio of flavin depletion signals, either *D(RBF)/D(FMN)* or *D(FMN)/D(RBF)*, is maximized. The reference case corresponds to the application of transform limited pulses. (From Ref. [4])

The present application of ODD utilizes a control field consisting of a shaped ultraviolet (UV) portion at 400 nm and a near infrared (IR) component at 800 nm, which is Fourier transform limited. The unshaped IR pulse follows the shaped UV pulse by a time delay τ, and the structure of the shaped UV pulse is deduced optimally under adaptive control to achieve ODD in the fluorescence signals from RBF and FMN. The primary operation of ODD relies on the shaped UV pulse coherently transferring ground state population into the flavin S_1 or S_2 excited states with the IR component likely creating further excitation of the molecules to higher lying S_n states. The IR field disrupts the vibronic excitation in S_1 or S_2 created

by the UV pulse in order to make a discriminating difference in the fluorescence spectra of RBF and FMN from S_1 recorded in the window 525–535 nm after a relaxation period of ~5 ns. Fluorescence is therefore depleted, and this fluorescence depletion value is used as measure of the molecular response to the field. The overall mechanism also may take advantage of any beneficial intra- and inter-molecular dynamical processes, and the ODD discrimination can draw on suitable coherent and incoherent aspects of the molecular dynamics.

In the first series of experiments the RBF and FMN solutions are in separate identical flow cells exposed to the same trial shaped UV pulse and time delayed unshaped IR pulse. An acousto-optic modulator is used to shape the UV pulses. A sequence of experiments $n = 1, 2,..$ was performed to record the relative depletion signal D_n

$$D_n(RBF) = \left[{F_n}^{und}(RBF) - {F_n}^{d}(RBF) \right] / {F_n}^{und}(RBF),$$

Where ${F_n}^{und}(RBF)$ is the undepleted fluorescence signal from the RBF cell (i.e., without application of the time delayed IR pulse) and ${F_n}^{d}(RBF)$ is the depleted signal in the presence of the IR pulse. An analogous expression applies to $D_n(FMN)$ for data collected from the FMN cell exposed to the same laser pulses.

The pulse shaper operated through phase modulation with 50 pixels, each on the range $0–2\pi$, over the bandwidth of the UV pulse (only 3–4 nm). A genetic algorithm of 30 individuals was used to optimize the UV pulse phases with convergence typically occurring in 100~300 generations.

Figure 5.3d demonstrates the ability of ODD to significantly draw apart the RBF and FMN fluorescence signatures in spite of their nearly identical linear optical spectra in Fig. 5.3b. For a given time delay τ, a specific optimal UV pulse is determined in the adaptive control experiment. The best discrimination was found for τ ~250–500 fs and the procedure was not able to find significant discrimination for $\tau \geq$ 1ps indicating a loss of coherence and/or insufficient overlap between the UV and IR pulses.

With a delay time τ typically around 250–500 fs, optimal pulse shapes found in different runs were very complex and showed considerable difference. They however produced exactly the same discrimination ratio when applying them, even weeks after the initial experiment. The underlying mechanisms are currently investigated, in order to identify whether this behaviour is generic or particular to this RBF/FMN system.

The assembled set of optimally discriminating laser pulses and their long-term stable performance permits exploiting ODD as a novel means for detection of nearly identical molecules when they are simultaneously present in a sample. In this work the recorded fluorescence depletion signals ${F_n}^{d}$ are utilized, as they are proportional to their respective flavin concentrations. Thus, the fluorescence signal F_n (mix) from a mixture of flavins generated with the n-th control UV-IR pulse pair is related to its

individual counterparts by

$$F_n(mix) = c(RBF)F_n{}^d(RBF) + c(FMN)F_n{}^d(FMN),$$

where *c(RBF)* is the fraction of RBF present and *c(RBF)* + *c(FMN)* = 1. The reference signals $F_n{}^d$*(RBF)* and $F_n{}^d$*(FMN)* are normalized to their respective concentrations deduced in learning the n-th control field, and similarly F_n is normalized to the total sum of the two flavins present. Two distinct ODD laser pulses could successfully determine the fractional content of the two flavins (the constrained relation between the fractions was not used in order to test the capabilities of ODD). Increasing the number of interrogating optimal pulses improves the standard deviation of the extracted component concentration fractions and a typical result using six pulses was *c(RBF)* = 0.35 ± 0.04 and *c(FMN)* = 0.68 ± 0.05 where the exact values were 0.33 and 0.66, respectively [4].

On a fundamental point of view, the exact molecular mechanisms underlying the selectivity allowed by the application of the optimally shaped pulses could be identified by quantum chemistry calculations [5]. It was shown that the optimal laser field makes use of low-frequency vibrational modes localized on the two biochromophores side chains (terminated by a phosphate group or by hydrogen) and selects the regions of their potential energy landscapes characterized by different transition dipole moments to higher excited states leading to different ionization probabilities. The resulting modulation of the excited state populations eventually controls the emitted fluorescence intensity.

5.4 Label-Free Identification of Peptides and Proteins

From the experimental standpoint, one of the major difficulties faced for the extension of the ODD scheme to proteins (or DNA) was the lack of deep UV (DUV) laser pulse shapers. This lack of ad hoc instrumentation motivated us to develop a dedicated MEMS based pulse shaper, in collaboration with CSEM-Neuchatel [21, 22]. This device proved successful for a very broad spectral range from the XUV [23] to the mid-IR.

First DUV-ODD experiments related to the fluorescing building blocks of proteins: Tryptophan and Tyrosine. The success of these experiments [24] enabled to identify tryptophan as ideal molecular target for performing ODD in proteins. In fact this bright emitting fluorophore displays a defined feature at short time-delays (<1 ps) that can be easily acted upon by an UV shaped femtosecond laser pulse and monitored by fluorescence depletion. Given tryptophan sensitivity to its local environment, it was decided to investigate the potential of ODD specifically on tryptophan-containing small peptides. We set-up a discrimination experiment aimed at the ODD fluorescence-based identification within several peptide pairs, otherwise showing identical fluorescence spectral and time-resolved response [25].

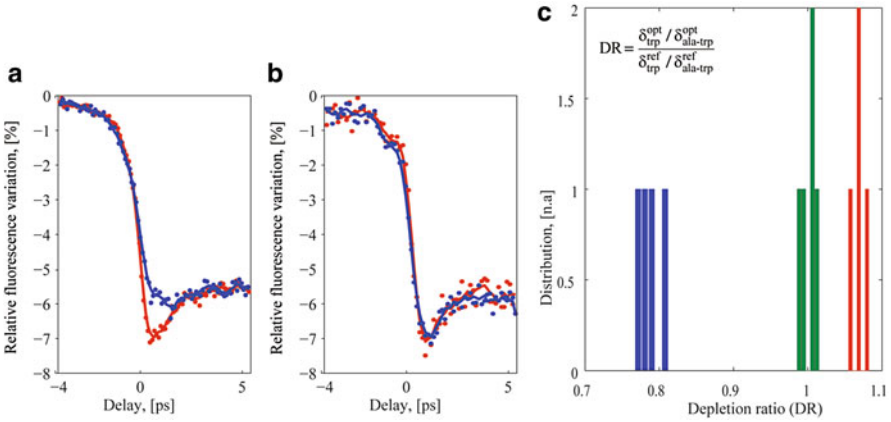

Fig. 5.4 Example of successful optimization for fluorescence depletion modulation in case of ala-trp (**a**) versus trp (**b**) with multi-objective algorithm optimization (**c**). Histogram of fluorescence depletions for ala-trp and trp. Green (middle column): reference obtained with Fourier-transform pulses, blue (left): maximization of fluorescencedepletion for ala-trp, red (right): maximization of fluorescence depletion for trp

A first series of feedback driven optimizations aimed at selectivity modifying the depletion amplitude at a given time delay (600 fs) of a defined peptide against another. An exemplary plot summarizing the outcome of an optimization run (ala-trp vs. trp) is shown in Fig. 5.4. In this case, a multi-objective optimization algorithm was launched with two independent goals: (i) increasing ala-trp fluorescence and (ii) decreasing trp fluorescence. One can appreciate the result of the procedure by applying the optimal mask on the two samples and acquiring the time resolved traces, as reported in Fig. 5.4a and b. In this example, the optimized pulse shape leads to an increase in the ala-trp time-resolved fluorescence variation by 20%, while trp remains unaffected. Optimization runs with the same objectives were repeated several times to evaluate statistical variations on the results. Note that different pulse shapes were found to lead to similar yields, pointing out the existence of multiple solutions.

The closed loop optimization procedure was then performed several times for the opposite set of goals, i.e. (i) decreasing ala-trp-fluorescence and (ii) increasing trp fluorescence. From the comparison of these traces with reference results obtained with Fourier transform pulses, we establish the histogram presented in Fig. 5.4c. The coherent manipulation of the molecular wavepacket leads to a variation of discrimination power that tears apart the trp and alatrp signatures by more than 8σ (where σ is the averaged statistical error on the results measured for a defined pulse shape).We also verified that the discrimination power DR was dependent on the time delay Δt. As expected for a coherent manipulation of the molecular wavepacket, DR decreases to zero for time delays larger than decoherence time (typically 1.5 ps).

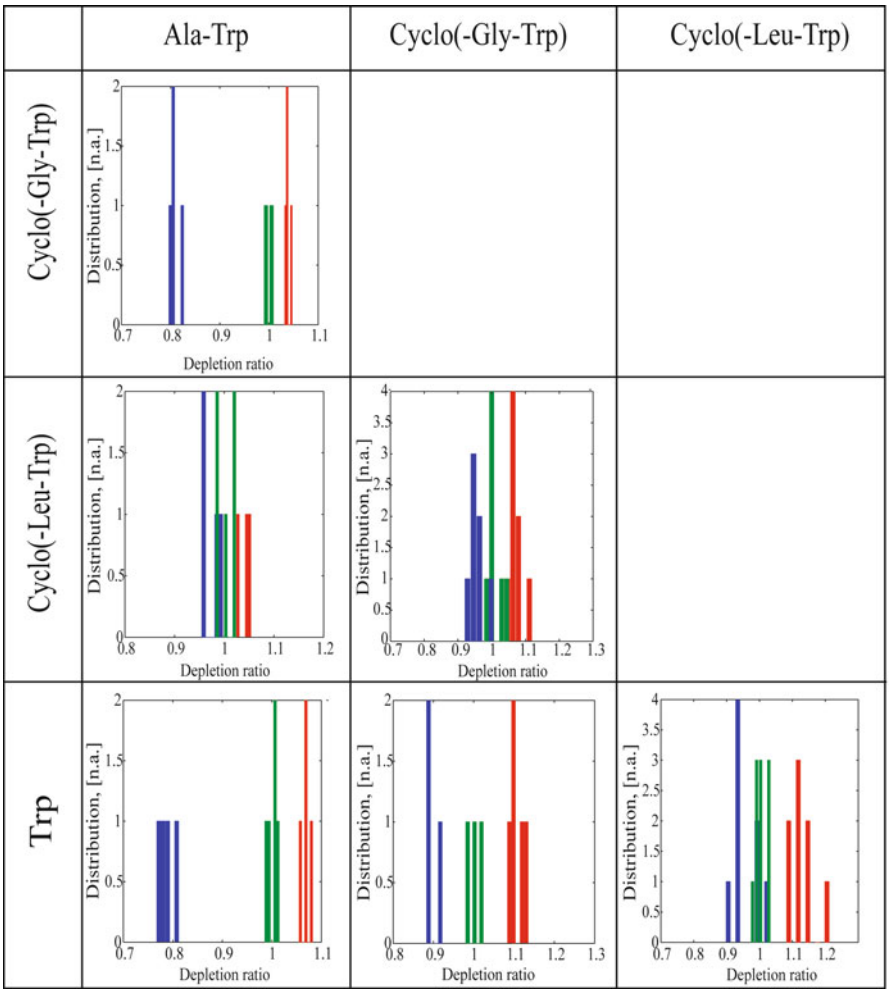

Fig. 5.5 Histograms of fluorescence depletions for various pairs of molecules. Green: reference obtained with Fourier-transform pulses, blue: maximization of fluorescence depletion for row molecule, red: maximization of fluorescence depletion for column molecule. (From Ref. [25])

The same procedure described above was applied to all pairs of dipeptides and free trp, giving rise to the matrix displayed in Fig. 5.5: In the histograms, bars indicate the ratios of the depletion values (row molecules over column molecules) obtained using phase-shaped DUV pulses retrieved by optimizations aimed at minimizing (blue) or maximizing (red) this quantity. Green bars correspond to the ratio of the depletion values measured with unshaped pulses. One can see that for several molecule pairs (trp vs. dipeptides, cyclo(-gly-trp) vs. ala-trp) the discrimination capability of the method is satisfactory, with a fluorescence difference between the optimized pulse shapes ranging from 3σ (trp vs. cyclo(-leu-

trp)) to 8σ (cyclo(-gly-trp) vs. ala-trp), which is remarkably high considering the modest bandwidth available for the shaped DUV pulse. This restricted parameter space does not allow, in opposite, to discriminate other dipeptides like cyclo(-leu-trp) vs. ala-trp.

It is clear from Fig. 5.5 that even for a group of very similar molecules addressed with identical experimental resources (laser spectral bandwidth as compared to absorption bandwidth, shaping spectral resolution), large variations do occur. No obvious reason emerged from our measurements. For instance, no correlation exists between the Stokes shifts in the static spectra and discriminability. Similarly, purely dynamical considerations, based on the time-resolved measurements, would suggest that, for instance, ala-trp should be more easily distinguished from cyclo(-leu-trp) (different relaxation time constants) than from free trp, which is not the case. No correlation with far infrared spectra was found either, stressing the importance of more complex quantum interference effects than just impulsive driving of vibrational modes.

As a natural follow up of this benchmark experiment, work is now in progress for transferring the DUV-ODD method to larger proteins with prospective applications in the field of label-free, consumable-free medical sensing. The goal of this undergoing study is currently, for instance, to quantify antibodies (such as IgG, 150 kDa) in blood serum, leading to first "quantum interference based bioassays" [6].

5.5 Quantum Controlled Vision in Live Animals?

The ultrafast investigation of the primary vision process (i.e., the rhodopsin-bound 11-cis-retinal to all-trans retinal isomerization upon photon absorption, Fig. 5.6) started with the pioneering paper by the Shank group where the arrival in the isomerization state in less than 100 fs was time-resolved using a transient absorption Scheme [26, 27]. Shortly after, Wang et al. showed wavepacket oscillations in this molecule demonstrating that coherence is preserved for at least 2 ps after photo-excitation despite the passage through the conical intersection leading to isomerization [27]. This molecular wavepacket is generated by a coherent superposition of a set of vibronic quantum states, and it evolves after excitation by the broadband femtosecond laser according to the field free Hamiltonian. The use of a second laser pulse, however, allows for the manipulation of the evolution of this wavepacket. For instance, Gerber's and Cerullo's groups demonstrated that it was possible to transfer the excited population back to the 11-cis ground state by stimulated emission before the transition through the conical emission takes place [28, 29]. These experiments can be seen as the first level of quantum control of the photo-isomerization of retinal in the rhodopsin protein.

The isomerization process can, however, be more precisely controlled by tailoring the shape of the molecular wavepacket itself. Modulating the amplitude and phase of the excitation laser spectral components allows, via the electric dipole interaction with the molecule, to modulate the phase and amplitude of the different

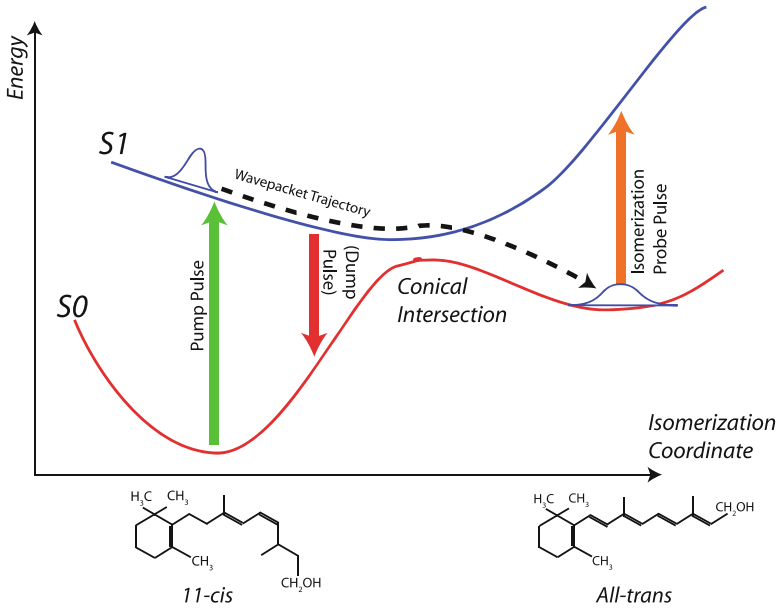

Fig. 5.6 Ultrafast manipulation of the retinal photo-isomerization in rhodopsin by pump-probe and pump-dump schemes acting on the excited states molecular wavepacket

excited wavefunctions, and thus the shape of the matter wavepacket. This concept of optimal quantum control was introduced by H. Rabitz and widely used since then for many applications in femtochemistry [10].

The first experimental demonstration of optimal quantum control of the retinal photo-isomerization in bacteriorhodopsin in solution was performed in 2005 by the group of R. Dwayne Miller [16, 30]. The experiment relied on the pump-probe scheme of Fig. 5.6 (without the dump pulse), in which the photoisomerization yield was probed by the red-shifted absorption from the isomer. The time delay between the pump and the probe during the pump pulse shape optimization procedure, was set 20 ps apart, in order to probe long term, stable isomerization. The authors showed that by applying an optimally shaped laser pulse, it was possible to increase the retinal's photo-isomerization yield by 20% as compared to a Fourier limited femtosecond pulse (Fig. 5.7 a–d). Conversely, an anti-optimal pulse shape reduced the photo-isomerization efficiency by 20%. Although a scientific debate about the linearity of the process followed these pioneering experiments, the basic concept of modulating the photo-isomerization with different pulse shapes was demonstrated. Successively, the Bucksbaum group set up a similar experiment confirming the sensitivity of isomerization to phase but only limited to pulses exceeding 10^{16} photons/cm^2 [17]. Although demonstrated on free bacteriorhodopsin in solution, these pioneering experiments set the groundwork for investigations on quantum controlling visual opsins.

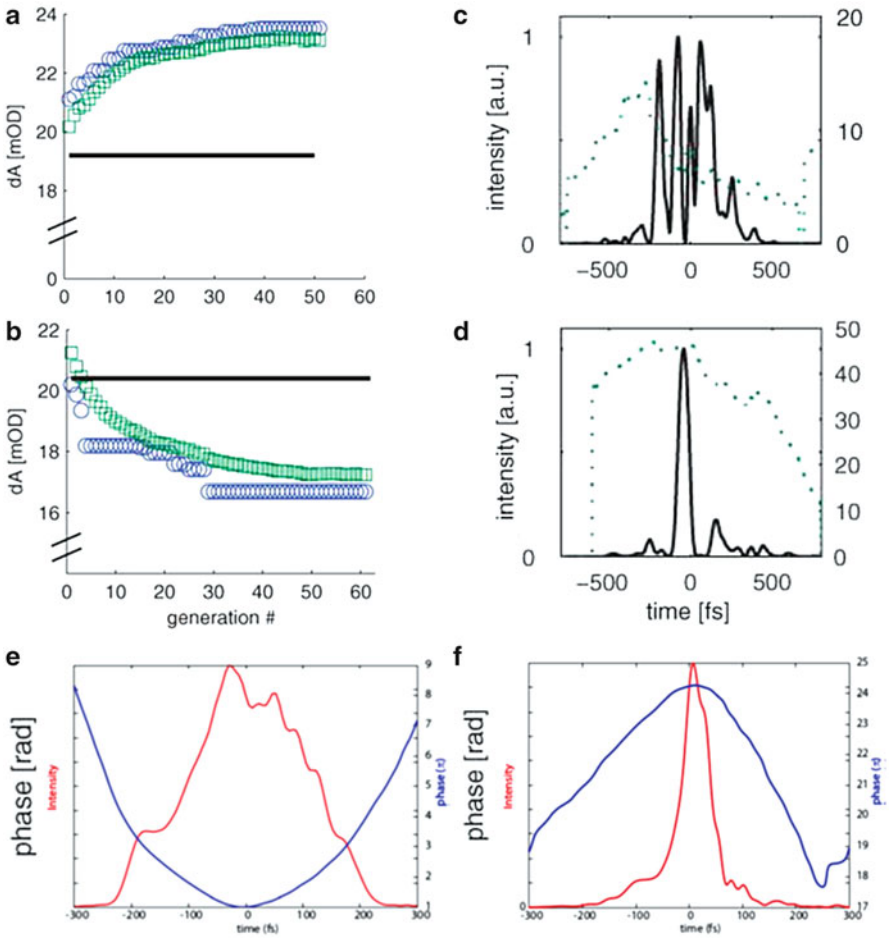

Fig. 5.7 Optimal quantum control of the photo-isomerization of retinal in bacteriorhodopsin. (**a**–**d**): Results from the original R.Dwayne-Miller paper [16]. (Adapted from Ref. 16). Optimization (**a**) and anti-optimization (**b**) procedure of the retinal photo-isomerization, leading to the pulse shapes in (**c** and **d**) respectively. These results were obtained by modifying the spectral amplitude as well. (**e**, **f**): results from our group, using different molecules, different lasers, different algorithms, and by modulating only the phase of the incoming pulse

These experiments also raised an active discussion about the possibility of controlling systems with single photon interactions, which is still ongoing [16, 31–37]. Two main topics emerged from these discussions: [1] whether, in open systems, the environment can contribute to a control in the linear regime, and [2] whether amplitude modulation and calibration flaws may lead to the original conclusions from the Dwayne-Miller group. In order to contribute to the latter part of the discussion, we reproduced the original experiment with a phase-only pulse shaper and precisely corrected for laser power fluctuations.

Interestingly, the spectral phase obtained by optimizations share several characteristics with the ones obtained by Dwayne Miller in that the pulse providing decreased isomerization bears a picosecond multi-peak structure, while the one leading to increased isomerization possess a temporal structure close to Fourier-transform.

More specifically, they realized a transient absorption measurement based on a shaped excitation pulse in the green (around 550 nm, 40 fs) and a weak probe pulse at 630 nm to measure the transition to the all-trans isomer. By using a genetic algorithm to retrieve the optimal phase-shape, the possibility to control the isomerization yield both for enhancing or decreasing the natural occurring yield (Fig. 5.7) was demonstrated [38].

However, these works were performed on bacteriorhodopsin in solution, and not rhodopsin from visiual pigments. These latter proteins are significantly different than bacteriorhodopsin, although both proteins are seven transmembrane serpentines and use retinal as their light substrate. The signaling pathways from photon absorption to neuron hyperpolarization are complex. The first step is always retinal photo-isomerization, which then induces a conformational change of rhodopsin and opsins and a cascade of reactions involving the activation of transducins (G proteins), followed by a cGMP phosphodiesterase, and eventually by the closure of cyclic nucleotide-gated Na + channels that trigger a hyperpolarization of the rod and cone cells, an ensuing depolarization of bipolar cells and the firing of retinal ganglion cells (Fig. 5.8).

A practical method to detect this activity is electroretinography (ERG), which measures electrophysiological activity of the retina (similar to electrocardiography). ERG is nowadays a widely used, noninvasive, electrophysiological assay of retinal function with well-documented methods of analysis [39]. We recently showed that it was possible to manipulate the photo-isomerization yield of photoreceptor molecules in a live mouse by modulating the spectral phase of a green femtosecond light pulse and record the electric signal generated by the retina. Our experiment is based on a kHz amplified Ti:Sapphire laser system coupled with a noncollinear parametric amplifier generating 50 fs pulses at 535 nm.

The visual response was acquired by three electrodes placed in contact with the irradiated eye, the forehead, and under skin in the tail (for ground voltage reference), respectively. First preliminary results are presented in Fig. 5.9. In these ERG traces, one can identify the characteristic A-wave (negative at early times) and B-wave (positive at later times) signals. The former is mainly attributed to cone activity and the latter to second-order retinal neurons from cones. These results unambiguously establish the possibility to efficiently acquire the visual response *in vivo* using pulsed ultra-short laser excitation, paving the way to possible quantum control of vision in living animals.

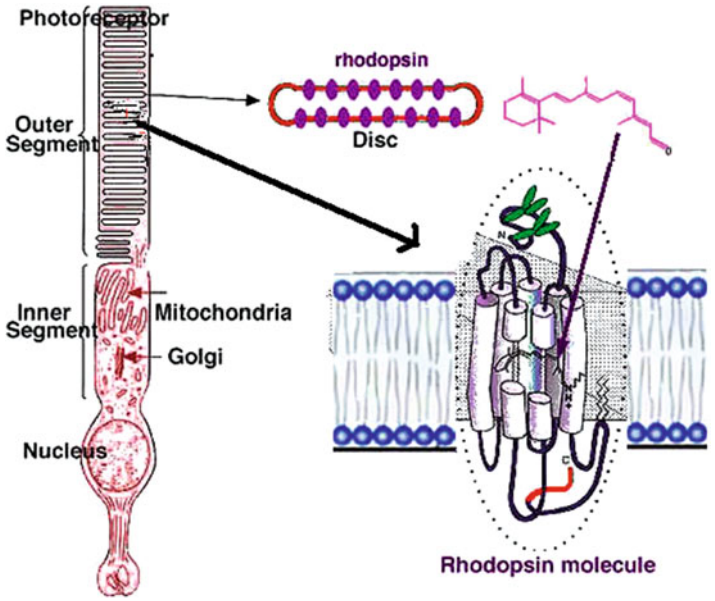

Fig. 5.8 Rod cell (left) showing a rhodopsin in outer segment disc membranes. (From webvision.med.utah.edu)

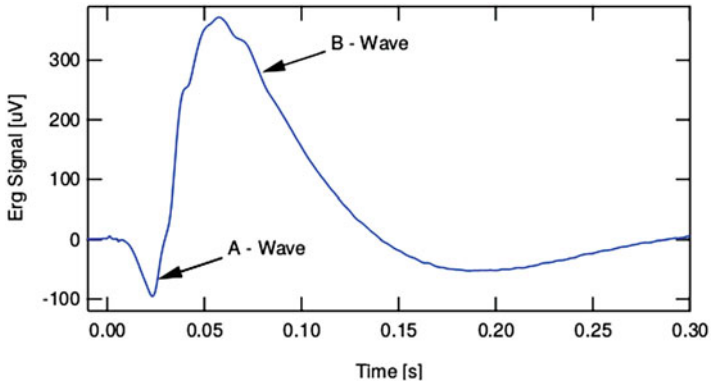

Fig. 5.9 Photopic A- and B-wave electro-retinogram (ERG) response recorded on a live C57BL/6 mouse, under illumination with a 40 fs, 535 nm laser. The A-wave amplitude and its implicit time reflect activity of M/L cones

5.6 Coherent Control of Nerve Firing in Living Brain Tissues

The photoisomerization of retinal within rhodopsin molecules acts as a photoswitch, which can be used for optically controlling nerve firing. With the advent of optogenetics, channel-rhodopsins (ChRh) of different types are expressed in cells

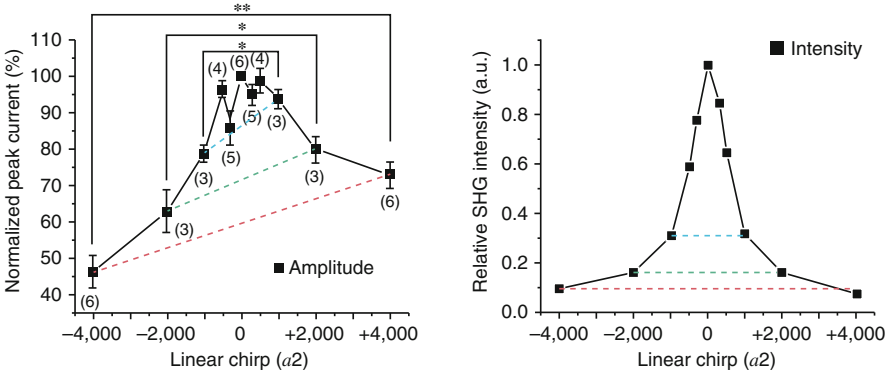

Fig. 5.10 **Left** Summary of normalized peak current amplitudes for negative and positive linear chirps. All currents were normalized to the phase-compensated condition ($a2 = 0\,\mathrm{fs}^2$). The numbers in parentheses refer to the number of neurons the currents were measured in at each linear chirp. Asterisks represent statistical significance: $^{*}p < 0.05$, $^{**}p < 0.005$. **Right**: SHG intensities at different linear chirp: $a2$ (in fs^2) $= \pm 4000$, ± 2000 and $\pm$ 1000. The SHG intensity at $a2 = 4000\,\mathrm{fs}^2$ is almost identical for PCH (0.075) and NCH (0.091); however, the peak current amplitudes in **c** are significantly different. (From Ref. [41])

from different genetically modified organisms, including mammals like mice. The optical control of brain neurons in these animals was demonstrated, e.g. for remotely controlling their muscular motion, but also for manipulating their behavior [40]. Alternatively, light stimulation and optogenetics may have significant applications in medicine, and in particular in neurodegenerative health issues, like Parkinson or Alzheimer diseases.

In 2017, a disrupting experiment was performed by the group of S. Boppart on coherent controlling living brain tissues [41]. More precisely, he induced 2-photons excitation of ChR2 and consecutive nerve firing and optimized the process while changing the spectral phase of the incoming 1 um wavelength pulses. The readout was performed electro-phisiologically with a patch clamp apparatus.

The authors observed clear asymmetry in chirp of the stimulation yield of the nerves, which is an indication of coherent effects in the photo-isomerization process in the retinal moiety (Fig. 5.10 left). Indeed, if a 2-photon excitation process is clearly favored by highest intensities, and thus short pulses, it should be equally efficient for negatively or positively chirped pulses of the same duration, as demonstrated for second harmonic generation (SHG) in Fig. 5.10 right.

The higher stimulation yield for positively chirped pulses than for negative ones points to some intra-pulse molecular processes involving the phase of the incoming field. A first interpretation attempt of this process, proposed by the authors, would be some kind of pump-dump effect for negatively chirped pulses (see Fig. 5.6) that would reduce the photo-isomerization yield by bringing back the population of the excited state to the ground state. However, in the present case, the excitation involves 2 photons, and the back stimulation would involve 2 photons as well, making this

explanation very unlikely. A clear explanation of these results is nowadays still lacking but reminds 2-photons quantum control results obtained on different dyes by the group of G. Gerber in the 2000s [14, 15].

On the practical point of view, two-photon opto-genetics is a very hot topic, as it allows targeting single cells with higher resolution and deeper stimulation as infrared radiation is much much less scattered and absorbed in tissue. The drawback of 2-photon stimulation is, however, the higher required intensity, which may be damageable for tissues. Increasing the yield of the process with quantum control is therefore particularly relevant.

5.7 Entangled Photons Microscopy

As mentioned in the introduction, another quantum signature than interference of states in the same system, is entanglement of different sub-systems. The most celebrated evidence of this process is the violation of Bell's inequalities in 1982 by the group of A. Aspect using entangled pairs of photons [42]. Since then these experiments set the ground to a "second quantum revolution", which involves all the properties of entangled states for applications like quantum cryptography, quantum telecommunications, quantum computers, or, more generally, what is called today "quantum technologies".

In entangled states, two subsystems (e.g. 2 photons) are linked in a common state, which means that if one of the subsystem is in a particular state, than the other one has to be in a particular state as well. Let's imagine 2 qubits A and B, which may have 2 values 0 and 1 (e.g. the polarization values of 2 photons A and B). Then these 2 qubits are entangled if they are represented, for example, by the following 2-particle (Bell) state:

$$\left|\Psi^{\pm}\right\rangle = \frac{1}{\sqrt{2}}\left(|0\rangle_A \otimes |1\rangle_B \pm |1\rangle_A \otimes |0\rangle_B\right).$$

These nonlocal connections between the subsystems A and B clearly have implications on the probabilities of detection, i.e. correlations, when experiments are performed. For instance, when the 2 photons cross a beamsplitter, they are known to bunch or anti-bunch, exhibiting clear non-classical statistics [43].

In microscopy, entangled states have recently been used to significantly enhance resolution and precision in phase contrast arrangements. Indeed, the minimal phase difference $\Delta\phi$ observable in a classical phase contrast microsocope scales with $N^{-1/2}$ while it scales with N^{-1} for entangled states (where N is the number of photons) [44]. Clearly, to improve phase resolution and beat the classical limit, N should be larger than 1. The above example of entangled particles above can be extended to

NOON states, where the subsystems A and B consist of N identical particles. For instance the NOON equivalent of the symmetric Bell state above writes:

$$|\psi_{\mathrm{NOON}}\rangle = \frac{|N\rangle_a|0\rangle_b + |0\rangle_a|N\rangle_b}{\sqrt{2}},$$

For a N = 2 NOON state, the quantum phase resolution would thus beat the classical limit by a factor $2^{-1/2}$. This was demonstrated by Ono et al. in their recent paper [44], as presented in Fig. 5.11, where the classical limit was experimentally beaten by 1.35 ± 0.12, i.e. close to the Heisenberg limit for 2 photons of $2^{-1/2}$. The phase object used in the experiment, a Q written on a glass plate, is only 17 nm high, demonstrating the potential of entanglement enhanced microscopy. To further improve the phase resolution, higher N "NOON state" sources would be required, which is still currently a major technological challenge.

5.8 Conclusion

Quantum inspired technologies are blooming in a wealth of domains. We presented some examples in biophotonics, covering both applicative technologies like microscopy, and more fundamental questions about the role of quantum physics in the natural evolution of organisms. There is no doubt that quantum biophotonics will represent a major field of activity in the next years. Whether purely quantum effects will be widely used for applications is unclear, but what was widely confirmed in the past, is that quantum concepts inspired groundbreaking advances in spectroscopy and photonics, even while using classical coherent light.

Acknowledgements The author gratefully acknowledge his collaborators at the Universities of Geneva and Lyon, in particular L. Bonacina, F. Courvoisier, L. Guyon, V. Boutou, E. Salmon, J. Yu, G. Mejean, J. Kasparian, C. Kasparian, A. Rondi, S. Afonina, J. Extermann, P. Bejot, S. Weber, D. Kiselev, J. Gateau, S. Hermelin and M. Moret, as well as H. Rabitz and his group at Princeton, particularly M. Roth and J. Roslund.

We also acknowledge the financial support of the Swiss National Science Foundation (contracts No. 2000021-111688 and No 200020-124689), and the Swiss NCCR MUST.

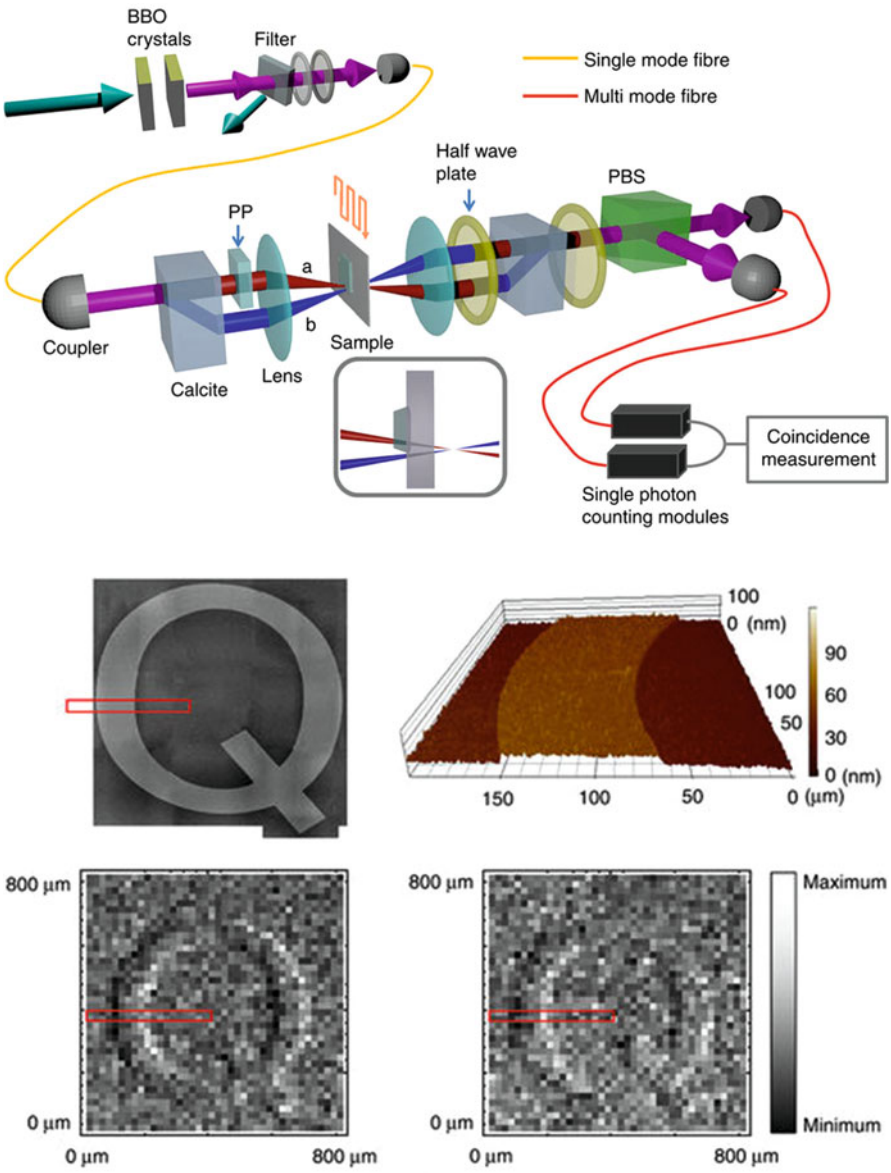

Fig. 5.11 **Upper**: Experimental set-up of the polarization entangled NOON microscope. **Lower:** results on a phase object representing a Q. The lower images clearly show the enhanced contrast as compared to classical light based phase contrast microscopy. (From Ref. [44])

References

1. Lambert N, Chen Y-N, Cheng Y-C, Li C-M, Chen G-Y, Nori F (2013) Nat Phys 9:10–18
2. Engel GS, Calhoun TR, Read EL, Ahn TK, Mancal T, Cheng YC, Blankenship RE, Fleming GR (2007) Nature 446(7137):782–786
3. Collini et al (2010) Nature 463:644–648
4. Roth M, Guyon L, Roslund J, Boutou V, Courvoisier F, Wolf JP, Rabitz H (2009) Phys Rev Lett 102:253001
5. Petersen J, Mitric R, Bonacic-Koutecky V, Wolf JP, Roslund J, Rabitz H (2010) Phys Rev Lett 105:073003
6. Afonina S, Gateau J, Staedler D, Bonacina L, Wolf J.P, in preparation (2018)
7. Tannor DJ, Kosloff R, Rice SA (1986) J Chem Phys 85:5805–5820
8. Tannor DJ, Rice SA (1985) J Chem Phys 83:5013–5018
9. Judson RS, Rabitz H (1992) Phys Rev Lett 68:1500–1503
10. Warren WS, Rabitz H, Dahleh M (1993) Science 259:1581–1589
11. Weiner AM (2000) Rev Sci Instrum 71:1929–1960
12. Bonacina L, Extermann J, Rondi A, Boutou V, Wolf JP (2007) Phys Rev A 76:023408
13. Dantus M, Lozovoy VV (2004) Chem Rev 104:1813–1859
14. Brixner T, Damrauer NH, Niklaus P, Gerber G (2001) Nature 414:57–60
15. Brixner T, Gerber G (2003) Chem Phys Chem 4:418–438
16. Prokhorenko VI, Nagy AM, Waschuk SA, Brown LS, Birge RR, Miller RJD (2006) Science 313:1257
17. Florean AC et al (2009) PNAS 106(27):10896–10900
18. Ventalon C, Fraser JM, Vos MH, Alexandrou A, Martin JL, Joffre M (2004) PNAS 101:13216–13220
19. Pastirk I, Dela Cruz JM, Walowicz KA, Lozovoy VV, Dantus M (2003) Opt Express 11:1695
20. Li BQ, Rabitz H, Wolf JP (2005) J Chem Phys 122:154103
21. Rondi A, Extermann J, Bonacina L, Weber S, Wolf J-P (2009) Appl Phys B 96:757–761
22. Weber SM, Bonacina L, Noell W, Kiselev D, Extermann J, Jutzi F, Lani S, Nenadl O, Wolf J-P, de Rooij NF (2011) Rev Sci Instrum 82:075106
23. Kiselev D, Kraus PM, Bonacina L, Wörner HJ, Wolf JP (2012) Opt Express 20(23):843–25849
24. Rondi A, Bonacina L, Trisorio A, Hauri C, Wolf J-P (2012) Phys Chem Chem Phys 14:9317–9322
25. Afonina S, Nenadl O, Rondi A, Bonacina L, Extermann J, Kiselev D, Dolamic I, Burgi T, Wolf JP (2013) App Phys B 111:541–549
26. Schoenlein R, Peteanu L, Mathies R, Shank CV (1991) Science 254(5030):412–415
27. Wang Q, Schoenlein RW, Peteanu LA, Mathies RA, Shank CV (1994) Science 266:422–424
28. Polli D et al (2010) Nature 467(7314):440–443
29. Vogt G, Nuernberger P, Brixner T, Gerber G (2006) Chem Phys Lett 433(1):211–215
30. Prokhorenko VI, Nagy AM, Miller RD (2005) J Chem Phys 122(18):184502
31. Joffre M (2007) Science 317:453
32. Liebel M, Kukura P (2017) Nat Chem 9:45
33. Brumer P, Shapiro M (1989) Chem Phys 139:221–228
34. Spanner M, Arango CA, Brumer P (2010) J Chem Phys 133: 151101(R)
35. Katz G, Ratner MA, Kosloff R (2010) New J Phys 12: 015003(R)
36. Arango CA, Brumer P (2013) J Chem Phys 138: 071104(R)
37. Weigel A, Sebesta A, Kukura P (2015) J Phys Chem Lett 6:4023–4037
38. El Hage K, Brickel S, Hermelin S, Gaulier G, Schmidt C, Bonacina L, van Keulen SC, Bhattacharyya S, Chergui M, Hamm P, Rothlisberger U, Wolf J-P, Meuwly M (2017) Struct Dyn 4:061507

39. McCulloch DL et al (2015) Doc Ophthalmol 130(1):1–12
40. Reardon S (2016) Nature News. https://doi.org/10.1038/nature.2016.20995
41. Paul K, Sengupta P, Ark ED, Tu H, Zhao Y, Boppart S (2017) Nat Phys 13:1111–1116
42. Aspect A, Grangier P, Roger G (1982) Phys Rev Lett 49:91–94
43. Hong CK, Ou ZY, Mandel L (1987) Phys Rev Lett 59(18):2044–2046
44. Ono T, Okamoto R, Takeuchi S (2013) Nat Commun 4:2426